

Article

Efficient and Selective Removal of Palladium from Simulated High-Level Liquid Waste Using a Silica-Based Adsorbent NTAamide(C8)/SiO₂-P

Jiaxuan Shi ¹, Junli Wang ^{1,2}, Wentao Wang ², Xuan Wu ², Hui Wang ^{2,*} and Jianwei Li ^{1,*}

¹ State Key Laboratory of Chemical Resource Engineering, College of Chemical Engineering, Beijing University of Chemical Technology, Beijing 100029, China

² Department of Radiochemistry, China Institute of Atomic Energy, Beijing 102413, China

* Correspondence: hwihwi@126.com (H.W.); lijw@mail.buct.edu.cn (J.L.)

Abstract: In order to realize the effective separation of palladium from high-level liquid waste (HLLW), a ligand-supported adsorbent (NTAamide(C8)/SiO₂-P) was prepared by the impregnation method in a vacuum. The SiO₂-P carrier was synthesized by in situ polymerization of divinylbenzene and styrene monomers on a macroporous silica skeleton. The NTAamide(C8)/SiO₂-P adsorbent was fabricated by impregnating an NTAamide(C8) ligand into the pore of a SiO₂-P carrier under a vacuum condition. The adsorption performance of NTAamide(C8)/SiO₂-P in nitric acid medium has been systematically studied. In a solution of 0.2 M HNO₃, the distribution coefficient of Pd on NTAamide(C8)/SiO₂-P was 1848 mL/g with an adsorption percentage of 90.24%. With the concentration of nitric acid increasing, the adsorption capacity of NTAamide(C8)/SiO₂-P decreases. Compared to the other 10 potential interfering ions in fission products, NTAamide(C8)/SiO₂-P exhibited excellent adsorption selectivity for Pd(II). The separation factor ($SF_{Pd/other\ metals} > 77.8$) is significantly higher than that of similar materials. The interference of NaNO₃ had a negligible effect on the adsorption performance of NTAamide(C8)/SiO₂-P, which maintained above 90%. The adsorption kinetics of Pd(II) adsorption on NTAamide(C8)/SiO₂-P fits well with the pseudo-second order model. The Sips model is more suitable than the Langmuir and Freundlich model for describing the adsorption behavior. Thermodynamic analysis showed that the adsorption of Pd(II) on NTAamide(C8)/SiO₂-P was a spontaneous, endothermic, and rapid process. NTAamide(C8)/SiO₂-P also demonstrated good reusability and economic feasibility.

Keywords: palladium(II); adsorption; high-level liquid waste; NTAamide(C8)/SiO₂-P adsorbent



Citation: Shi, J.; Wang, J.; Wang, W.; Wu, X.; Wang, H.; Li, J. Efficient and Selective Removal of Palladium from Simulated High-Level Liquid Waste Using a Silica-Based Adsorbent NTAamide(C8)/SiO₂-P. *Nanomaterials* **2024**, *14*, 544. <https://doi.org/10.3390/nano14060544>

Academic Editor: Vincenzo Vaiano

Received: 29 January 2024

Revised: 8 March 2024

Accepted: 13 March 2024

Published: 20 March 2024



Copyright: © 2024 by the authors. Licensee MDPI, Basel, Switzerland. This article is an open access article distributed under the terms and conditions of the Creative Commons Attribution (CC BY) license (<https://creativecommons.org/licenses/by/4.0/>).

1. Introduction

Nuclear energy, as a clean and reliable energy source, is favored by many countries due to its unique advantages. High-level liquid waste (HLLW) generated from fuel treatment contains more than 40 elements, such as Ru, Rh, Pd, Tb, Tc, Cs, Sr, Mo, I, etc. [1,2] Palladium is a platinum-group metal with a silver luster. The palladium in the HLLW includes stable isotopes ¹⁰⁴Pd (17 wt.%), ¹⁰⁵Pd (29 wt.%), ¹⁰⁶Pd (21 wt.%), ¹⁰⁸Pd (12 wt.%), and ¹¹⁰Pd (4 wt.%), and radioactive isotope ¹⁰⁷Pd (17 wt.%). The half-life of ¹⁰⁷Pd is 6.5 × 10⁶ years. Compared with other elements in HLLW (such as Rh and Ru), the radioactivity is very weak and considered safe to recover [3–5]. During the subsequent treatment of HLLW through vitrification, palladium tends to deposit at the bottom of the furnace because of its high melting point and low solubility in the high-level radioactive nuclear waste glass, which greatly reduces the stability of the glass body and increases the difficulty of vitrification. To enhance the vitrification efficiency, palladium needs to be extracted from HLLW in advance. On the other hand, due to the excellent catalytic properties, thermal stability, corrosion resistance, and other characteristics of palladium, it is an important strategic material with economic and industrial value [6,7] and has been widely used in

catalysis [8], actor manufacturing [9], aerospace [10], automobile [11], biomedicine [12], and other aspects. Palladium, like other platinum group metals, has a scarce reserve, and its supply always requires secondary resources [13]. Comprehensive treatment of secondary resources and efficient recycling of Pd are of great significance to increase the supply of Pd and promote the sustainable development of multiple industries [14–17]. Therefore, recovering palladium from HLLW not only facilitates the subsequent treatment of HLLW through vitrification, but also makes use of the secondary resources to generate Pd.

Solvent extraction is a widely used method for recovering palladium from HLLW [1,2,18,19]. It is well known that Pd(II) belongs to a soft Lewis acid, and can easily complex with the ligand containing a soft-donor N or S atom [20]. *N,N,N',N',N'',N''*-hexaoctyl-nitrilotriacetamide (NTAamide(C8)) has received increasing attention, as a new soft non-heterocyclic N-donor extractant. The structure of NTAamide(C8) is shown in Figure 1. Sasaki et al. [21] used NTAamide(C8) to recover Pd(II) through extraction electrodeposition, and the extraction rate could reach above 91% in all cycles. Wang et al. [22] studied the extraction ability of NTAamide(n-Oct) for Pd(II) and confirmed its good selectivity, extraction efficiency, and loading capacity. Sasaki et al. [23] studied the extraction behavior of NTAamide(C8) for 70 metals and found that the extraction rate for Pd(II) was the highest, indicating that NTAamide(C8) had good selectivity for Pd(II) and could be used to separate Pd(II) from multi-element mixed solutions, such as HLLW.

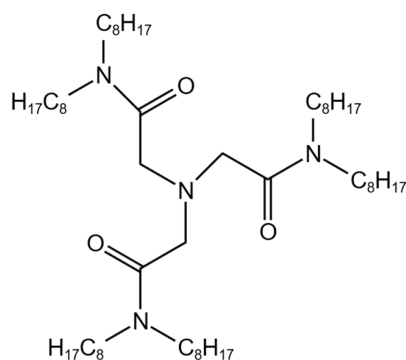


Figure 1. Structure of NTAamide(C8).

Despite the high recovery efficiency and the potential to scale up, solvent extraction methods suffer from emulsification and prominent three-phase problems. The extraction process also consumes a large volume of solvents and generates toxic organic waste. In addition, solvent extraction has high requirements for subsequent treatment and economic investment. Due to these drawbacks, some alternative separation methods have been developed [24–28]. The chemical adsorption method [25,28,29] is widely used due to its high efficiency and low cost, especially for recovery metals at low concentrations. At present, the adsorbents mainly include inorganic material adsorbents, nanomaterial adsorbents, ion exchange resin adsorbents, and biomaterial adsorbents. Awual et al. [30] prepared a highly selective and efficient adsorbent by immobilizing the synthesized *N,N*-bis(salicylidene)1,2-bis(2-aminophenylthio)ethane ligand onto mesoporous silica monoliths, and its maximum sorption capacity for Pd(II) ions was 163.13 mg/g. Mincke et al. [31] synthesized three chitosan derivatives and used them to recover Pd(II) and Pt(IV) from acidic solutions. These adsorbents showed high adsorption rates, reaching equilibrium within 30 min. Their maximum adsorption capacities for Pd(II) were 262.6 mg/g, 154.7 mg/g, and 340.3 mg/g, respectively. However, due to the coexistence of platinum group metals in HLLW and their similar chemical properties, adsorbents tend to adsorb them simultaneously, making it impossible to selectively adsorb Pd. This needs further in-depth study.

SiO₂-P is a composite carrier composed of porous silica and organic copolymers. The adsorbents based on SiO₂-P demonstrate a high adsorption rate, good reusability, and environmental friendliness. Yu et al. [32] prepared a macroporous silica polymer (TRPO/SiO₂-P) to recover scandium from sulfuric acid solutions. The adsorption was selective, reaching

an equilibrium within 120 min with a saturated adsorption of approximately 13.3 mg/g. Ning et al. [33] used silica-based isoBu-BTP/SiO₂-P adsorbent to separate Ru, Rh, and Pd from nitrate solution, and their saturated adsorption capacities reached 0.37 mmol/g, 0.34 mmol/g, and 0.71 mmol/g, respectively. Su et al. [34] prepared a silica-based polymer adsorbent (isopentyl-BTBP/SiO₂-P) by a maceration method in a vacuum for efficient and continuous separation of Pd from complex systems. In a HNO₃ solution of 3 M, the distribution coefficient of Pd was 5226 mL/g, and the maximum adsorption capacity was 31.7 mg/g.

Considering the advantages of NTAamide(C8) extractant and SiO₂-P carrier, this study aims to combine them to prepare a new adsorption material, which is expected to achieve high selectivity and adsorption percentage simultaneously. The adsorption performance and mechanism of recovery of palladium ion from simulated HLLW were investigated.

2. Materials and Methods

2.1. Chemicals

Nitric acid was supplied by Sinopharm Chemical Reagent Co., Ltd. (Beijing, China). Rhodium nitrate was provided by Kunming Bosen Precious Metal Materials Processing Co., Ltd. (Kunming, China). The standard solutions of Gd, Ho, Dy, Ce, Sn, Re, Sm, Pr, Tb, Mo, and Sr were obtained from Guobiao Testing & Certification Co., Ltd. (Beijing, China). All chemicals were of analytical grade. Deionized water was obtained through a Smart-Q15 system (Hitech Instruments Co., Ltd. Shanghai, China) in the lab. Palladium nitrate dihydrate, ruthenium nitrosyl nitrate, and other chemicals were purchased from Shanghai Macklin Biochemical Co., Ltd. (Shanghai, China). All chemicals were analytical grade.

2.2. Material Preparation

2.2.1. Preparation of SiO₂-P

The inorganic organic composite carrier SiO₂-P was prepared by an in situ polymerization method [35,36]. The preparatory flow sheet of the SiO₂-P is illustrated in Figure 2. First, the stabilizers in styrene and divinylbenzene were removed by vacuum distillation and washed with a dilute alkali solution, respectively. Porous SiO₂ was added to the round-bottom flask of a rotary evaporator, and the flask was rotated at 40 rpm. The air in the flask was displaced by first vacuuming and then purging with inert gases. The air pressure was reduced to 3 kPa again. Acetophenone and diethyl phthalate were used as diluents and placed in a beaker. Then, the monomers (divinylbenzene and styrene) were added to the beaker and mixed thoroughly, followed by adding initiator AIBN and V-40. Then, the mixture was poured into the round-bottom flask to fully mix with SiO₂. Inert gas was introduced to ensure that the device is in an oxygen-free environment. The co-polymerization reaction started between styrene and divinylbenzene upon heating. After the reaction was completed, the product SiO₂-P was washed and dried before use.

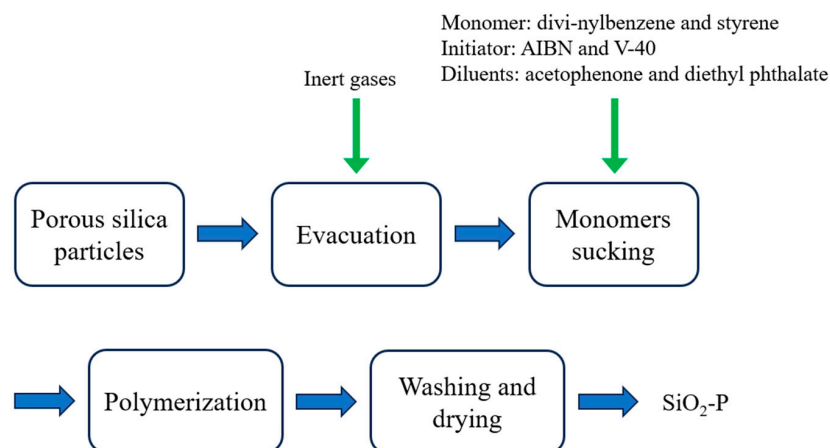


Figure 2. Preparatory flow sheet of SiO₂-P.

2.2.2. Preparation of NTAamide(C8)/SiO₂-P

NTAamide(C8) ligand was loaded onto the SiO₂-P carrier by the impregnation method in a vacuum [37–39]. The preparatory flow sheet of the NTAamide(C8)/SiO₂-P is illustrated in Figure 3. First, an appropriate amount of methanol was added to SiO₂-P and mixed thoroughly, followed by solid–liquid separation. The above steps were repeated three times, and then the obtained SiO₂-P was dried. SiO₂-P (10 g) was placed in a round-bottom flask. Then, 5 g of NTAamide(C8) was dissolved in an appropriate amount of dichloromethane and transferred to the round-bottom flask. The flask was rotated at 100 rpm on a rotary evaporator at room temperature and pressure for 1 h, and then left standing for 1 h. The flask was subsequently heated in a water bath to 310 K while maintaining the rotation speed at 100 rpm for 1.5 h before turning on the cooling water circulation device. After the above steps, the vacuum pump was turned on to slowly depressurize the extractant into the channel of SiO₂-P until the diluent dichloromethane was completely volatilized. After drying, the NTAamide(C8)/SiO₂-P was obtained.

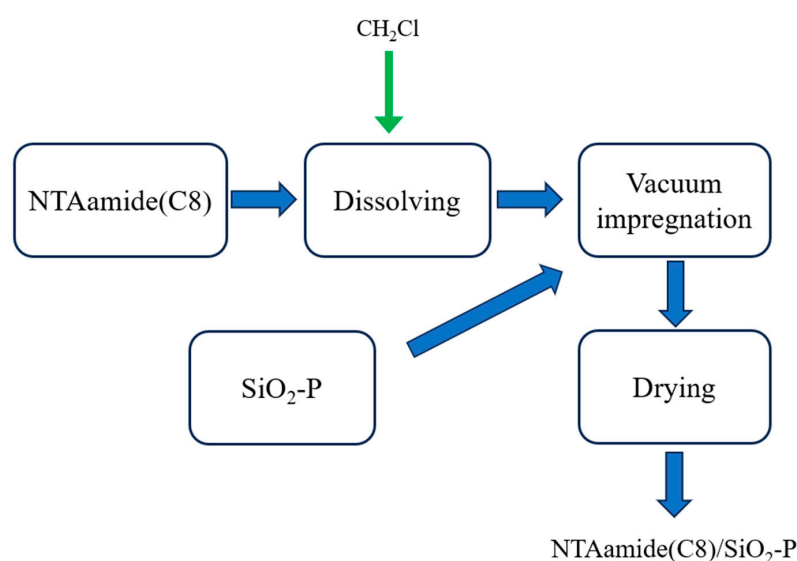


Figure 3. Preparatory flow sheet of NTAamide(C8)/SiO₂-P.

2.3. Material Characterization

The morphology and composition of the composites were measured by scanning electron microscopy (SEM, Hitachi S4800, Hitachi Ltd., Tokyo, Japan) equipped with an energy dispersive spectrometer (EDS). Thermogravimetric (TG) analysis of the composites was conducted using a thermal analyzer (TGA/DSC3+, Mettler-Toledo International Inc., Zurich, Switzerland). The structural parameters were measured using the Brunauer–Emmett–Teller method (BET; ASAP2460, Micromeritics instrument (Shanghai) Ltd., Shanghai, China). X-ray diffraction (XRD) was performed on a diffractometer (Ultima IV, Rigaku Beijing Corporation, Beijing, China). An X-ray photoelectron spectrometer (XPS; ESCALAB 250, Thermo Fisher Scientific, Waltham, MA, USA) was used to characterize the surface properties. Fourier transform–infrared spectroscopy (FT-IR) spectra were collected on an FT-IR spectrometer (Nicolet 6700, Thermo Fisher Scientific, Waltham, MA, USA). The content of metal ions in the solution was measured by an inductively coupled plasma emission spectrometer (ICP-OES; JY2000-2, Horiba instruments (Shanghai) Co., Ltd., Shanghai, China).

2.4. Adsorption Experiments

A certain amount of the adsorbent was mixed with the metal ion solutions (0.01–1 M) in a centrifuge tube, which was placed in a constant-temperature water bath and oscillated at 280 rpm. After the adsorption reached equilibrium, the mixture was centrifuged and the supernatant was used to analyze the concentration of metal ions by ICP-OES. The acidity of the solution, the dosage of the adsorbent, the concentration of metal ions, the temperature,

and the coexisting ions were adjusted to evaluate the static adsorption performance of the adsorption material. Several important physical parameters such as adsorption capacity (Q , mg/g), adsorption percentage (E), distribution coefficient (K_d , mL/g), and separation factor (SF) are defined as follows:

$$Q = \frac{(C_0 - C) \cdot V}{m} \quad (1)$$

$$E = \frac{(C_0 - C) \cdot V}{C_0} \times 100\% \quad (2)$$

$$K_d = \frac{(C_0 - C)}{C_0} \cdot \frac{V}{m} \quad (3)$$

$$SF_{A/B} = \frac{K_{dA}}{K_{dB}} \quad (4)$$

where C_0 and C (mg/L) represent the initial and equilibrium metal ion concentrations, respectively, m (g) is the mass of the adsorbent, and V (mL) is the volume of the aqueous phase. A and B represent two different components in the same aqueous phase.

3. Results and Discussions

3.1. Characterization

To determine the morphology and elemental mapping of the adsorbent, SEM characterization was performed. The SEM results of NTAamide(C8)/SiO₂-P and the SEM-EDS results of Pd-loaded NTAamide(C8)/SiO₂-P are shown in Figure 4. The surface of the NTAamide(C8)/SiO₂-P sphere is relatively rough, which indicates that NTAamide(C8) entered the inner pores of SiO₂-P. The uniform distribution of N elements indicates that NTAamide(C8) was uniformly loaded onto SiO₂-P. The results after adsorption show that Pd elements are evenly distributed on the surface of the sphere, confirming the adsorption of Pd.

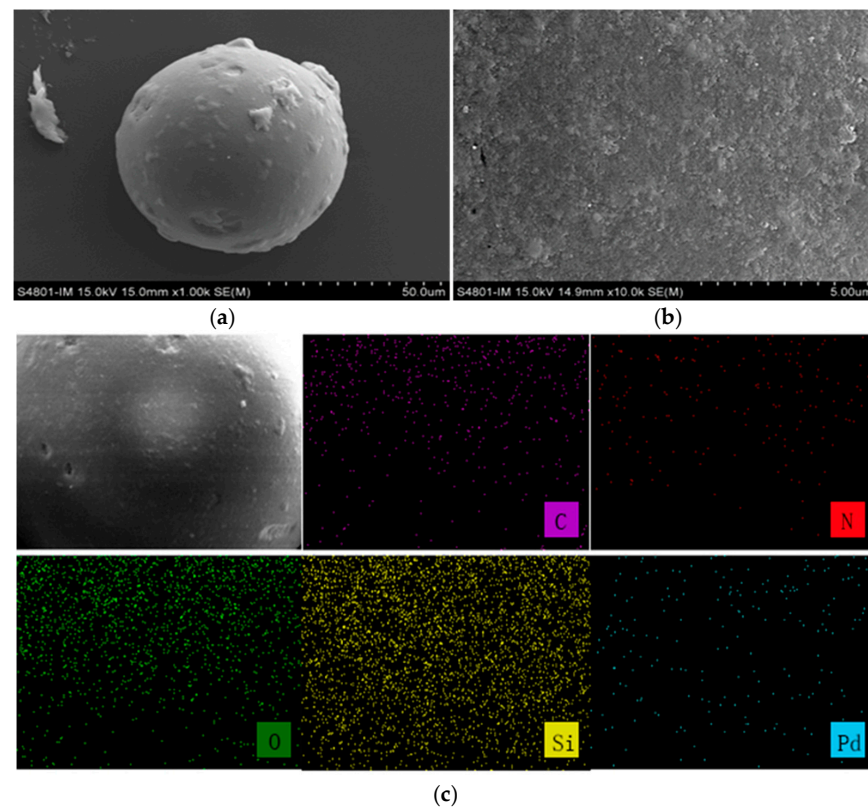


Figure 4. (a,b) SEM images of NTAamide(C8)/SiO₂-P; (c) SEM-EDS images of Pd-NTAamide(C8)/SiO₂-P.

The SEM results of SiO₂-P are shown in Figure S1. In addition, the organic content of NTAamide(C8) in NTAamide(C8)/SiO₂-P was determined to be 35.63% through a TG thermal analyzer (Figure S2). By analyzing N₂-adsorption–desorption isotherm and pore diameter distribution, it was calculated that the BET surface area is 26.4 m²/g, pore volume is 0.17 cm³/g, and the average pore diameter is 29.4 nm (Figure S4 and Table S1).

3.2. Adsorption Experiments

3.2.1. Effect of HNO₃ Concentration

The effects of HNO₃ concentration on the adsorption of Pd(II) by NTAamide(C8)/SiO₂-P and SiO₂-P were studied (Equation (2)). As shown in Figure 5, NTAamide(C8)/SiO₂-P exhibits a strong affinity for Pd(II) at a low acid concentration (0.2 M). The adsorption of Pd(II) decreases with the increasing HNO₃ concentration. At a high HNO₃ concentration, the protonated N donor with positive charges tend to repel Pd(II) ions, significantly reducing the adsorption percentage. Compared with carrier SiO₂-P, the adsorption capacity of NTAamide(C8)/SiO₂-P was greatly increased. The experiments of NTAamide(C8)/SiO₂-P were repeated three times with an error of less than 1.5%.

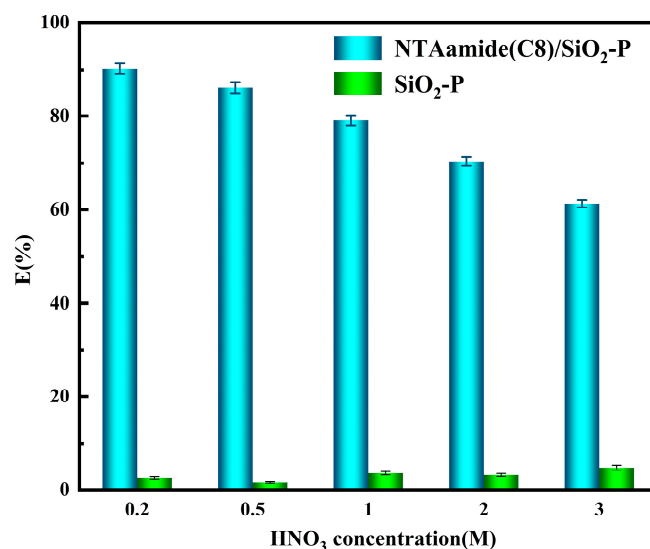


Figure 5. Effects of HNO₃ concentration on the adsorption percentage of Pd(II) onto NTAamide(C8)/SiO₂-P and SiO₂-P. (C₀: 1 mM, *m/v*: 0.05 g/10 mL, Temperature: 298 K, and *r*: 280 rpm).

3.2.2. Effect of NTAamide(C8)/SiO₂-P Dosage

As shown in Figure 6, with the increasing dosages of NTAamide(C8)/SiO₂-P, the adsorption percentage of Pd increases. When 80 mg of NTAamide(C8)/SiO₂-P is added, the adsorption percentage reaches 98.41% (Equation (2)). More adsorbents provide more adsorption sites for Pd(II), resulting in a lower equilibrium concentration and higher adsorption percentage.

3.2.3. Selectivity of NTAamide(C8)/SiO₂-P

The adsorption selectivity of NTAamide(C8)/SiO₂-P was studied (Figure 7). In 0.2 M nitric acid, NTAamide(C8)/SiO₂-P has no obvious adsorption effect on 10 metal ions. Comparatively, the distribution coefficient of Pd (Equation (3)) is significantly higher, suggesting that NTAamide(C8)/SiO₂-P has good adsorption selectivity ($SF_{Pd/other\ metals} > 77.8$ (Equation (4)) and can be used to separate Pd from other metal ions. NTAamide(C8)/SiO₂-P was compared with two similar materials. Me₂-CA-BTP/SiO₂-P [37] is a novel silica-based adsorbent, which is prepared to separate minor actinides from fission products in HLLW. The K_d of Pd is below 100 mL/g and $SF_{Am/Pd}$ value is 17 in 0.1 M HNO₃. IsoBu-BTP/SiO₂-P [33] has good adsorption capacity for Pd, but also adsorbs a large amount of Ru and Rh. It is unable to selectively separate Pd. Compared with these adsorptions,

NTAamide(C8)/SiO₂-P has superiority in selectivity. NTAamide(C8) has nitrogen donor atoms at the center of the backbone. In the HSAB (Hard-Soft-Acid-Base) framework, NTAamide(C8) is classified as a soft base. Among these metal ions, Pd is the only soft acid with good electron acceptance ability. Pd(II) can coordinate with the ligands through nitrogen donor atoms on the central frame and carbonyl groups.

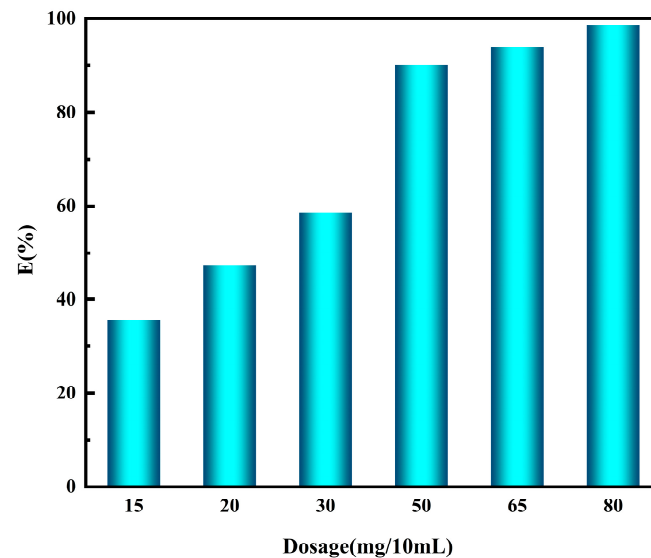


Figure 6. Effect of NTAamide(C8)/SiO₂-P dosage on the adsorption percentage of Pd(II). (C_0 : 1 mM, C_{HNO_3} : 0.2 M, Temperature: 298 K, and r : 280 rpm).

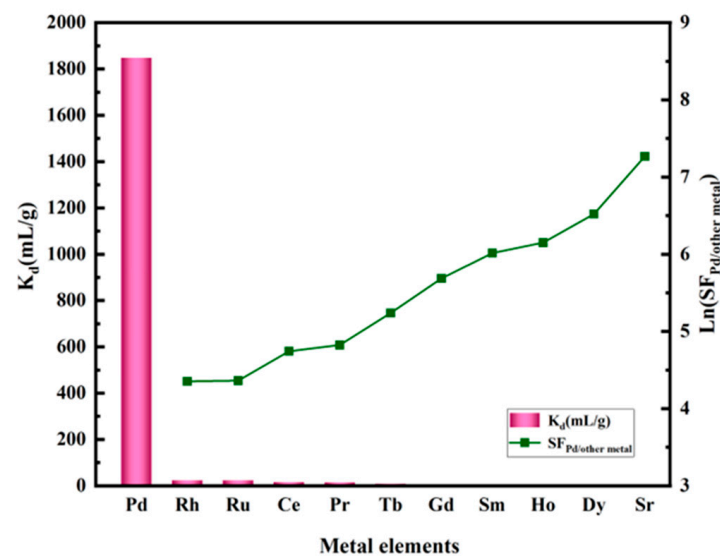


Figure 7. Adsorption of 11 typical metal ions onto NTAamide(C8)/SiO₂-P (C_0 : 1 mM, C_{HNO_3} : 0.2 M, m/v : 0.05 g/10 mL, Temperature: 298 K, and r : 280 rpm).

3.2.4. Effect of NaNO₃ Concentration on Adsorption Performance

During the adsorption process, the N donor is protonated, requiring nitrate ions to maintain the charge balance. Therefore, the effect of sodium nitrate on the adsorption was investigated. The concentration of NaNO₃ varies from 0 to 5 M, and the adsorption of Pd(II) by NTAamide(C8)/SiO₂-P was studied in 0.2 M nitric acid (Figure 8). The system without NaNO₃ can achieve a high adsorption percentage. The presence of NaNO₃ slightly improves the adsorption percentage of NTAamide(C8)/SiO₂-P. The highest adsorption percentage (92.4%) is achieved when the NaNO₃ concentration is 2 M, which is about 2.2%

higher than the system without NaNO₃. Considering that NaNO₃ has a negligible effect on adsorption, the system without NaNO₃ is used for subsequent experiments.

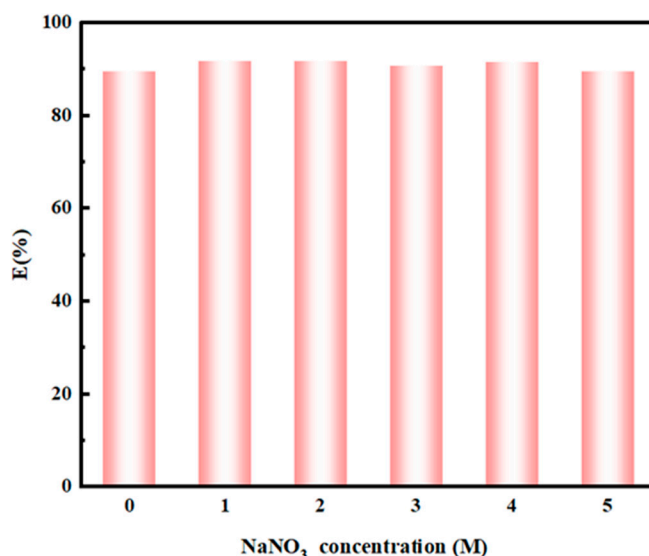


Figure 8. Effect of NaNO₃ concentration on the adsorption of Pd(II) onto NTAamide(C8)/SiO₂-P (C₀: 1 mM, C_{HNO₃}: 0.2 M, *m/v*: 0.05 g/10 mL, temperature: 298 K, and *r*: 280 rpm).

3.2.5. Adsorption Kinetics

The kinetics of Pd(II) adsorption on NTAamide(C8)/SiO₂-P was studied at 298 K. Pseudo-first order kinetics (Equation (5)) and pseudo-second order kinetics (Equation (6)) were used to fit the curves of adsorption capacity vs. time.

$$\ln(Q_e - Q_t) = \ln Q_e - k_1 \cdot t \tag{5}$$

$$\frac{t}{Q_t} = \frac{t}{Q_e} + \frac{1}{k_2 \cdot Q_e^2} \tag{6}$$

where Q_e and Q_t (mg/g) (Equation (1)) represent the equilibrium adsorption capacity and adsorption capacity at time t (min), respectively; k_1 (min⁻¹) and k_2 (mg/(g·min)) represent the adsorption rate constants of pseudo-first and pseudo-second order kinetics, respectively.

Their non-linear form is described as Equations (7) and (8), respectively:

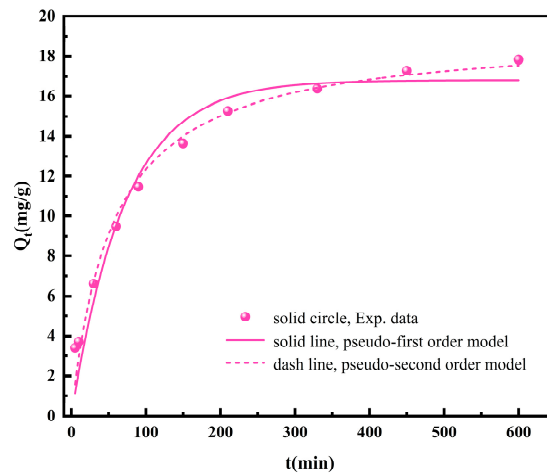
$$Q_t = Q_e \left(1 - e^{-k_1 \cdot t}\right) \tag{7}$$

$$Q_t = \frac{k_2 \cdot Q_e^2 \cdot t}{1 + k_2 \cdot Q_e \cdot t} \tag{8}$$

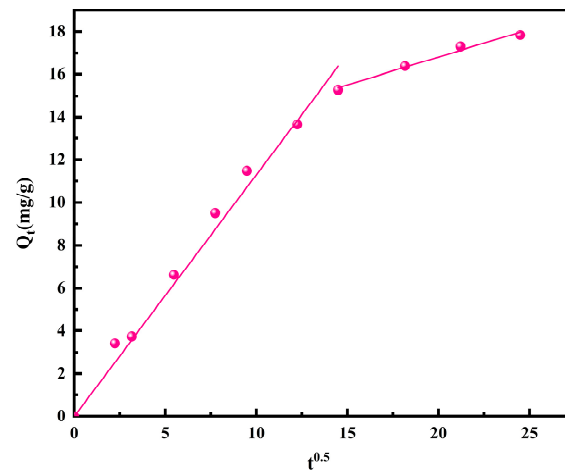
As shown in Figure 9a and Table 1, the pseudo-second order model has a higher correlation coefficient (R^2), and its theoretical equilibrium adsorption capacity (Q_e) is closer to the experimental value ($Q_{e,exp}$), suggesting it is more suitable to describe the adsorption process. The correlation coefficient was fitted through the formula. It indicates the degree of agreement between the experimental data and the model.

Table 1. Kinetics parameters of Pd(II) adsorption on NTAamide(C8)/SiO₂-P.

Pseudo-First-Order Model			Pseudo-Second-Order Model			Intraparticle Diffusion Kinetic Model		
K ₁	Q _e	R ²	K ₂	Q _e	R ²	K _{id}	C	R ²
0.0139	16.8	0.957	9.38 × 10 ⁻⁴	19.2	0.982	0.261	11.6	0.983



(a)



(b)

Figure 9. (a) Non-linear pseudo-first order, pseudo-second order kinetic, and (b) intraparticle diffusion model fitting for Pd(II) adsorption onto NTAamide(C8)/SiO₂-P. (C_0 : 1 mM, C_{HNO_3} : 0.2 M, m/v : 0.05 g/10 mL, Temperature: 298 K, and r : 280 rpm).

In order to explain the diffusion mechanism, the intraparticle diffusion model (Equation (9)) was applied to the experimental data [40]:

$$Q_t = k_{id}t^{0.5} + C \quad (9)$$

where k_{id} ($\text{mg}/(\text{g}\cdot\text{min}^{0.5})$) represents the intraparticle diffusion rate constant and the value of C is affected by boundary layer thickness.

As shown in Figure 9b and Table 1, the plots present two steps. The first step was surface diffusion stage and the second step was intraparticle diffusion stage. The plot did not pass through the origin, indicating that intraparticle diffusion is not the only rate-determining step. The decrease in slope indicates that the adsorption sites were occupied, and the adsorption rate decreased. The adsorption gradually reached equilibrium.

3.2.6. Adsorption Isotherm

By changing the initial concentration of Pd in the solution, the adsorption isotherm at 298 K, 303 K, 308 K, 313 K, and 318 K were measured. Five adsorption isotherm models (Langmuir, Freundlich, Temkin, Dubinin–Radushkevich, and Sips (Equations (10)–(14)))

were used to fit the experimental data to understand the relationship between adsorption capacity (Q) and Pd equilibrium concentration (Figure 10 and Table 2). From Table 2, the R² of the Sips isotherm model is higher than those of the other four isotherm models. Therefore, the Sips isotherm model is more suitable for describing the adsorption behavior of Pd(II) on NTAamide(C8)/SiO₂-P. The Sips isotherm is a combination of the Langmuir and Freundlich isotherm models, and it is based on the Freundlich equation assumption [40]. It is speculated that the adsorption of palladium is through a multi-molecular layer chemical process. 1/n is the Sips isotherm exponent, which can be used to indicate the non-uniformity of adsorption sites. If 1/n < 1, the adsorption sites on the adsorbent surface are not uniformly distributed. The Sips isotherm model also indicates a finite limit on adsorption capacity. The theoretical saturated adsorption capacity of NTAamide(C8)/SiO₂-P is higher than that of a similar material IONP@SiO₂ (6.5 mg/g) [41].

$$Q_e = \frac{Q_m \cdot K_L \cdot C_e}{1 + K_L \cdot C_e} \tag{10}$$

$$Q_e = K_F \cdot C_e^{\frac{1}{n}} \tag{11}$$

$$Q_e = B \ln A + B \ln C_e \tag{12}$$

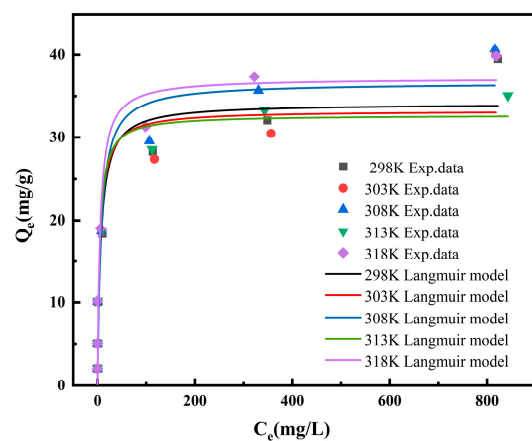
$$Q_e = Q_m \exp(-K_{DR} \epsilon^2) \tag{13}$$

$$Q_e = \frac{Q_m (K_S \cdot C_e)^{\frac{1}{n}}}{1 + (K_S \cdot C_e)^{\frac{1}{n}}} \tag{14}$$

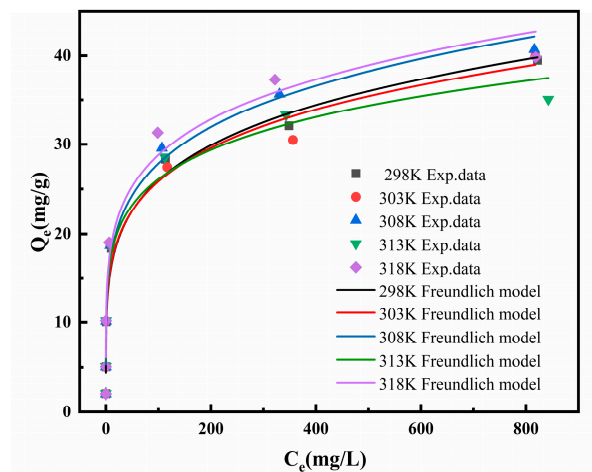
where Q_e and Q_m (mg/g) (Equation (1)) represent the equilibrium and theoretical saturated adsorption capacity, respectively, K_L (L/mg), K_F (mg¹⁻ⁿ·Lⁿ/g), K_{DR} (mol²/kJ⁻²), and K_S (mg^{1/n}/L^{1/n}) represent the model constants of Langmuir, Freundlich, Dubinin–Radushkevich, and Sips adsorption isotherm models, respectively, and n is adsorption intensity. A and B are Temkin constants, B = RT/b. Polanyi potential ε = RTln(1 + 1/C_e).

Table 2. Isotherm parameters of Pd(II) adsorption on NTAamide(C8)/SiO₂-P.

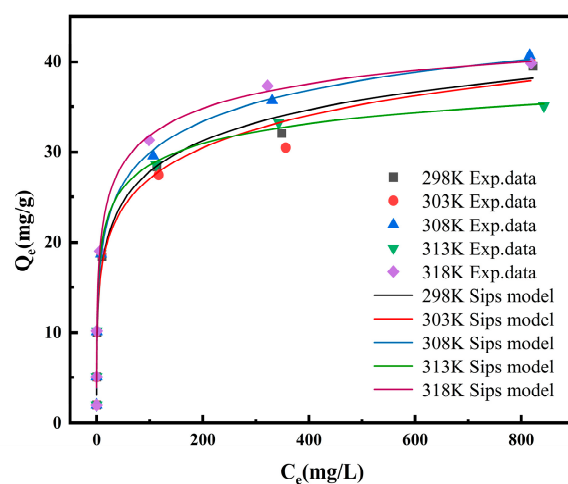
T	Langmuir Isotherm			Freundlich Isotherm		
	K _L	Q _m	R ²	K _F	n	R ²
298 K	0.150	34.1	0.903	10.2	4.93	0.985
303 K	0.185	33.3	0.870	10.5	5.11	0.977
308 K	0.136	36.6	0.902	11.2	5.07	0.985
313 K	0.222	32.7	0.901	11.9	5.87	0.973
318 K	0.184	37.1	0.913	12.2	5.34	0.965
	Temkin isotherm			D-R model		
	A	B	R ²	K _{DR}	Q _m	R ²
298 K	41.8	3.43	0.965	7.12 × 10 ⁻⁸	25.3	0.762
303 K	54.1	3.32	0.966	3.07 × 10 ⁻⁸	24.5	0.736
308 K	50.7	3.61	0.983	4.09 × 10 ⁻⁸	27.1	0.788
313 K	149.2	2.95	0.984	1.56 × 10 ⁻⁸	24.3	0.728
318 K	61.29	3.63	0.974	2.14 × 10 ⁻⁸	27.1	0.770
	Sips isotherm					
	K _S	Q _m	n	R ²		
298 K	4.62 × 10 ⁻³	63.2	3.19	0.993		
303 K	5.73 × 10 ⁻⁴	84.0	3.84	0.980		
308 K	6.22 × 10 ⁻³	64.6	3.22	0.995		
313 K	4.40 × 10 ⁻²	46.1	3.06	0.994		
318 K	3.54 × 10 ⁻²	52.1	2.80	0.987		



(a)



(b)



(c)

Figure 10. (a) Langmuir, (b) Freundlich, and (c) Sips isotherm fitting for Pd(II) adsorption onto NTAamide(C8)/SiO₂-P. (C_{HNO_3} : 0.2 M, m/v : 0.05 g/10 mL, and r : 280 rpm).

3.2.7. Adsorption Thermodynamics

To understand the thermodynamics of NTAamide(C8)/SiO₂-P adsorption and clarify the relationship between the adsorption and temperature, the adsorption isotherm experiments were conducted at 298–318 K, and the thermodynamic calculation was carried out by the Van't Hoff equation (Equations (15) and (16)).

$$\ln K_F = -\frac{\Delta H^\theta}{RT} + \frac{\Delta S^\theta}{R} \tag{15}$$

$$\Delta G^\theta = \Delta H^\theta - \Delta S^\theta \cdot T \tag{16}$$

where K_F is the model constant of the Freundlich adsorption isotherm model. ΔG^θ , ΔH^θ , and ΔS^θ are the changes in Gibbs free energy (J/mol), enthalpy (J/mol), and entropy (J/(K·mol)), respectively. R is the universal gas constant (8.314 J/(K·mol)).

Although the R^2 of the Sips isotherm model is higher, the deviation of K_s is relatively large. The Sips isotherm model is based on the Freundlich equation assumption, and the R^2 value of the Freundlich isotherm model is close to that of Sips. Therefore, K_F of the Freundlich adsorption isotherm model was used for the thermodynamic calculation.

The calculation results are shown in Figure 11 and Table 3. A positive ΔH value indicates that the adsorption of Pd(II) is an endothermic reaction, which is consistent with the adsorption isotherm experiments (the equilibrium adsorption capacity increases with the temperature). The ΔG value remains negative at different temperatures, indicating that the adsorption of NTAamide(C8)/SiO₂-P is a spontaneous process. The ΔS value is 44.5 J/K·mol for the adsorption process, suggesting that the adsorption is driven by entropy.

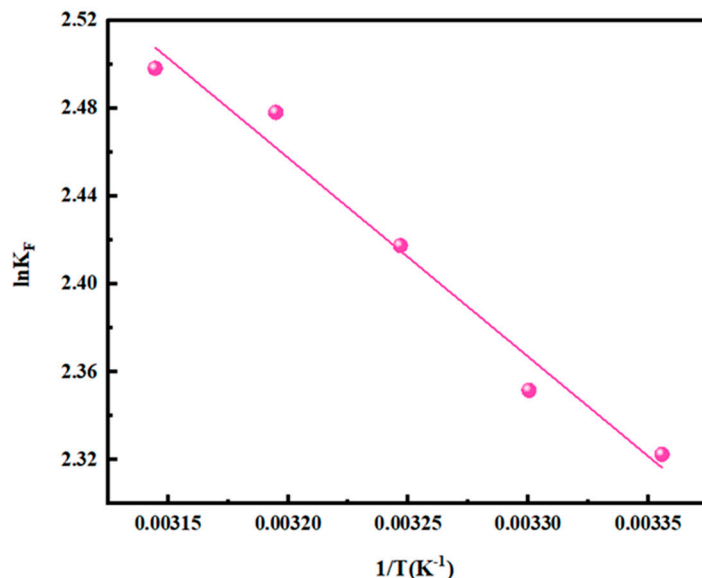


Figure 11. Thermodynamics fitting for Pd(II) adsorption onto NTAamide(C8)/SiO₂-P.

Table 3. Adsorption thermodynamic parameters of NTAamide(C8)/SiO₂-P. ($R^2 = 0.974$).

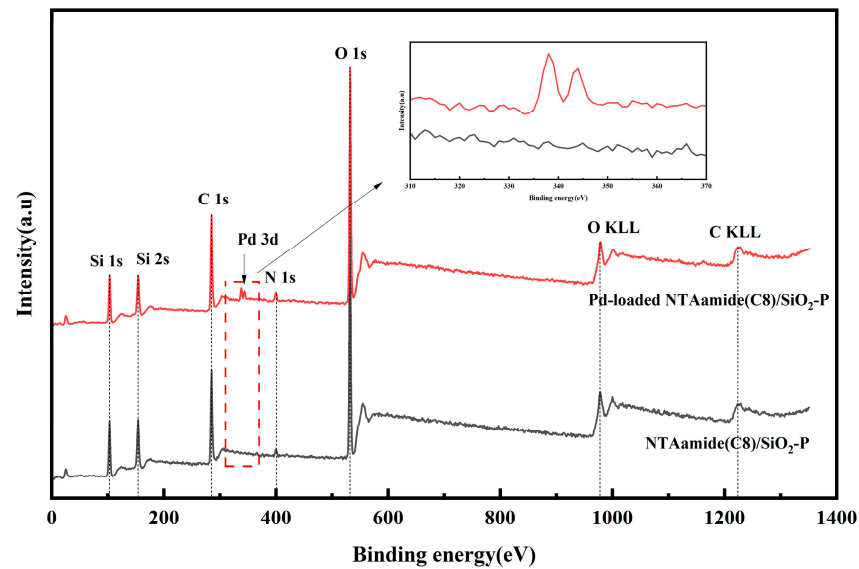
ΔH (J/mol)	ΔS (J/(K·mol))	ΔG (J/mol)				
		298 K	303 K	308 K	313 K	318 K
7.53×10^3	44.5	-5.73×10^3	-5.95×10^3	-6.18×10^3	-6.40×10^3	-6.62×10^3

3.3. Adsorption Mechanism

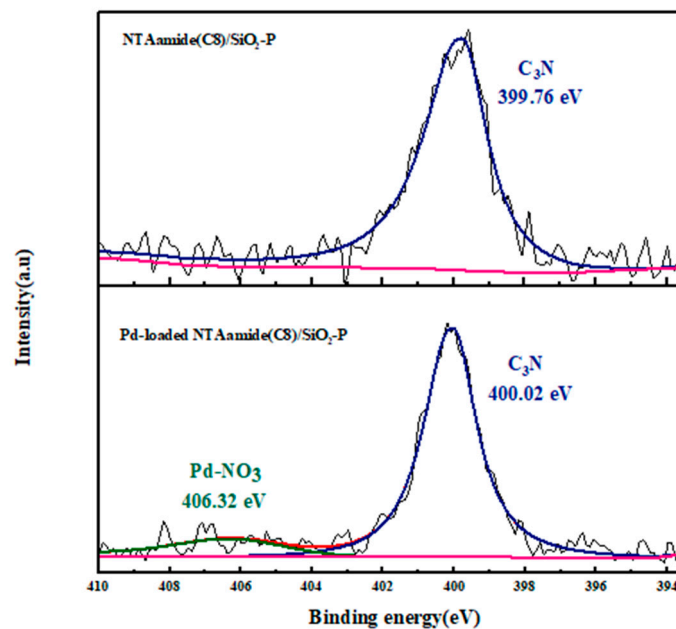
The interaction mechanism of NTAamide(C8)/SiO₂-P was studied using XPS and FT-IR.

The XPS spectra of NTAamide(C8)/SiO₂-P and Pd-loaded NTAamide(C8)/SiO₂-P are shown in Figure 12a. The presence of C1s, N1s, and O1s peaks and the two Auger peaks of

C and O in the spectrum is consistent with the composition of NTAamide(C8)/SiO₂-P. The N1s peak emerges at 400 eV, indicating that NTAamide(C8) has been loaded onto SiO₂-P. A characteristic peak of Pd3d is found at 338 eV after adsorption, indicating that Pd has been adsorbed by NTAamide(C8)/SiO₂-P. The XPS spectra of N1s is shown in Figure 12b. For NTAamide(C8)/SiO₂-P and Pd-loaded NTAamide(C8)/SiO₂-P, the binding energy of C₃N are 399.76 eV and 400.02 eV, respectively. The change in binding energy of C₃N implies that it may play an important role in the adsorption behavior. The specific mechanism will be further studied through FT-IR.



(a)



(b)

Figure 12. (a) XPS spectra of NTAamide(C8)/SiO₂-P and Pd-loaded NTAamide(C8)/SiO₂-P, (b) high resolution scans of N 1s spectrum before and after adsorption.

The FT-IR spectra of NTAamide(C8)/SiO₂-P and Pd-loaded NTAamide(C8)/SiO₂-P are shown in Figure 13. The characteristic peak at 798cm⁻¹ corresponds to the stretching vibration of Si-O, while the peaks at 470 and 1108 cm⁻¹ are associated with the stretching vibrations of Si-O-Si. The out-of-plane deformation vibration of the aromatic hydrocarbon (=C-H) is observed at 700 and 1462 cm⁻¹. The characteristic peaks at 1380 cm⁻¹ and 1650 cm⁻¹ correspond to the deformation vibration of the methyl group (CH₃) and the stretching vibration of C=O in NTAamide(C8). The stretching vibration peaks of methylene (C-H) in NTAamide(C8) appear at 2856 and 2927 cm⁻¹. The wide peak at 3450 cm⁻¹ is due to the vibration of H-O-H in water that has not been completely removed. NTAamide(C8) contains a tertiary amine structure (R₃N), which exhibits double peaks at 1230~1030 cm⁻¹. However, due to the stronger characteristic peak of Si-O-Si at 1108 cm⁻¹, the double peaks become a wider peak. After adsorption, the characteristic peaks are slenderer, indicating that the tertiary amine structure may coordinate with Pd(II), which is consistent with the composition of NTAamide(C8)/SiO₂-P. According to the relative literature [22,42], the 2:1 ligand/Pd²⁺ complexes were formed in a low concentration of HNO₃ solution. Two NTAamide(C8) ligand molecules coordinated with one four-coordinated Pd²⁺ via one of the three carbonyl groups and the central N atom, forming a complex cation. There are two NO₃⁻ ions anion as the counterpart ions for charge balance, and the NO₃⁻ ions only have a salting-out effect on the ligands under this condition [22]. The single peak originally located at 1650 cm⁻¹ was split into two peaks at 1650 and 1595 cm⁻¹, which is also consistent with the adsorption mechanism.

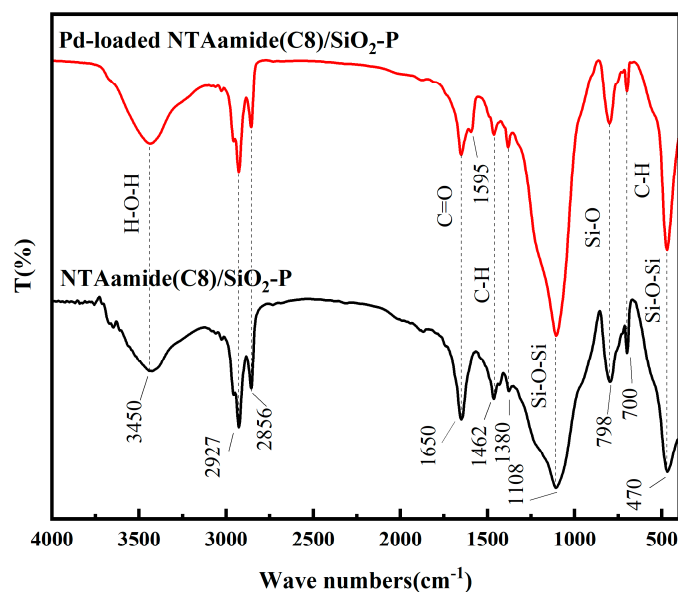


Figure 13. FT-IR spectra of NTAamide(C8)/SiO₂-P and Pd-loaded NTAamide(C8)/SiO₂-P.

NTAamide(C8) has nitrogen donor atoms at the center of the backbone. In the HSAB (Hard-Soft-Acid-Base) framework, NTAamide(C8) is classified as a soft base. Pd(II) can coordinate with the extractant through nitrogen donor atoms on the central frame and carbonyl groups. NO₃⁻ is required to participate in the reaction to maintain charge balance.

3.4. Reusability

Reusability is an important factor in evaluating the performance of adsorbents. The reusability of NTAamide(C8)/SiO₂-P was studied through six cycles of adsorption and desorption. First, 50 mg of the adsorbent was added to the Pd solution to reach adsorption equilibrium under certain conditions, and then the solution was removed. After drying, the used adsorbent was desorbed in a mixed solution of thiourea (0.01 M) and nitric acid (0.1 M) at 298 K while shaking at 280 rpm. As shown in Figure 14, the adsorption

percentage after six adsorption–desorption cycles was 82.92% (a decrease of approximately 7.3% from the original value). The solid–liquid separation operation during the experiment may result in a slight loss of the adsorbent, which can lead to a decrease in adsorption percentage. Therefore, the NTAamide(C8)/SiO₂-P adsorbent has good reusability, making the adsorption process economically feasible. The experiments were repeated three times with an error of less than 2.2%.

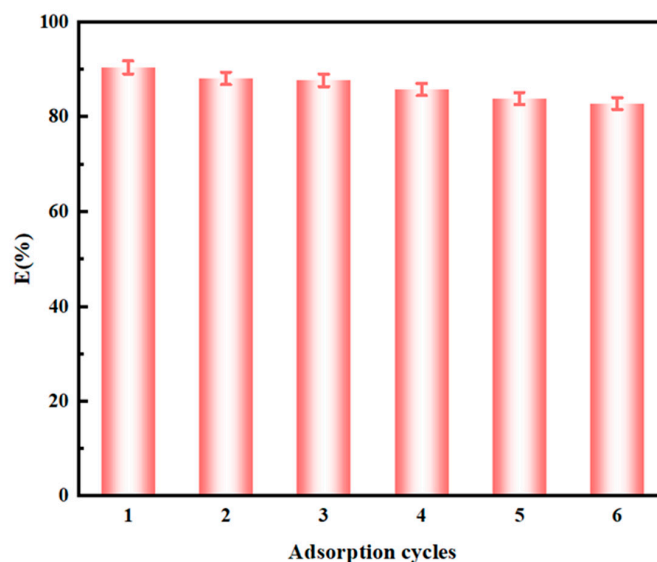


Figure 14. The reusability of NTAamide(C8)/SiO₂-P (C_0 : 1 mM, C_{HNO_3} : 0.2 M, m/v : 0.05 g/10 mL, Temperature: 298 K, and r : 280 rpm).

4. Conclusions

In this research, a mesoporous silica-based composite, NTAamide(C8)/SiO₂-P, was prepared by the impregnation method in a vacuum. The resulting NTAamide(C8)/SiO₂-P could adsorb Pd(II) efficiently in a nitric acid system. The results indicate that low acidity is conducive to the adsorption of Pd(II), with the uptake rate over 90%. In 0.2 M HNO₃ solution, NTAamide(C8)/SiO₂-P exhibits excellent adsorption selectivity for Pd(II) ($SF_{\text{Pd}/\text{other metals}} > 77.8$). The adsorption thermodynamics study has shown that the adsorption of Pd(II) on NTAamide(C8)/SiO₂-P is a spontaneous and endothermic process. Its adsorption kinetics matched well with the pseudo-second order kinetics model and the adsorption isotherm data met well with Sips model. After adsorption, thiourea desorption can be used to separate Pd(II), making NTAamide(C8)/SiO₂-P an excellent material for recovering Pd(II) from HLLW. It indicates the potential practicability of NTAamide(C8)/SiO₂-P in application. Finally, XPS and FT-IR results revealed the coordination mechanism in Pd adsorption. NTAamide(C8)/SiO₂-P has excellent adsorption selectivity and capacity and excellent reusability, meaning it has great application prospects in Pd separation. pH has a significant impact on the adsorption performance of NTAamide(C8)/SiO₂-P, and it is expected to be improved in the future. Although SiO₂-P is an excellent carrier, there are many other carriers that may contain a larger specific surface area or larger loading capacity. Replacing the carrier may improve the performance of the adsorbent.

Supplementary Materials: The following supporting information can be downloaded at: <https://www.mdpi.com/article/10.3390/nano14060544/s1>.

Author Contributions: Conceptualization, J.S. and J.W.; data curation, J.S. and X.W.; formal analysis, J.S. and J.W.; investigation, J.S. and J.W.; methodology, J.W.; project administration, H.W. and J.L.; resources, J.W. and W.W.; supervision, J.L.; validation, J.S. and J.W.; visualization, J.S.; writing—original draft, J.S.; writing—review and editing, J.S. and J.W. All authors have read and agreed to the published version of the manuscript.

Funding: This research received no external funding.

Data Availability Statement: Data are contained within the article.

Conflicts of Interest: The authors declare no conflict of interest.

References

1. Ruhela, R.; Tomar, B.S.; Sharma, J.N.; Seshagiri, T.K.; Adya, V.C.; Hubli, R.C.; Suri, A.K. Studies on the Separation and Recovery of Palladium from Simulated High Level Liquid Waste (SHLW) Solution with Novel Extractant *N,N,N',N'*-tetra (2-ethylhexyl) Dithiodiglycolamide DTDGA. *Sep. Sci. Technol.* **2013**, *48*, 1049–1055. [[CrossRef](#)]
2. Ruhela, R.; Sharma, J.N.; Tomar, B.S.; Adya, V.C.; Sheshgiri, T.K.; Hubli, R.C.; Suri, A.K. *N,N,N',N'*-Tetra(2-Ethylhexyl) Thiodiglycolamide T(2EH)TDGA: A Promising Ligand for Separation and Recovery of Palladium from High Level Liquid Waste (HLLW) Solutions. *Sep. Sci. Technol.* **2011**, *46*, 965–971. [[CrossRef](#)]
3. Ruhela, R.; Singh, A.K.; Tomar, B.S.; Hubli, R.C. Separation of palladium from high level liquid waste—A review. *RSC Adv.* **2014**, *4*, 24344–24350. [[CrossRef](#)]
4. Zha, M.; Liu, J.; Wong, Y.-L.; Xu, Z. Extraction of palladium from nuclear waste-like acidic solutions by a metal–organic framework with sulfur and alkene functions. *J. Mater. Chem. A* **2015**, *3*, 3928–3934. [[CrossRef](#)]
5. Kumaresan, R.; Jain, R.; Venkatesan, K.A.; Antony, M.P.; Bhanage, B.M. Extraction and electrochemical behavior of fission palladium in room-temperature ionic liquid. *J. Radioanal. Nucl. Chem.* **2014**, *303*, 1047–1052. [[CrossRef](#)]
6. Yakoumis, I.; Panou, M.; Moschovi, A.M.; Panyas, D. Recovery of platinum group metals from spent automotive catalysts: A review. *Clean. Eng. Technol.* **2021**, *3*, 100112. [[CrossRef](#)]
7. Hughes, A.E.; Haque, N.; Northey, S.A.; Giddey, S. Platinum Group Metals: A Review of Resources, Production and Usage with a Focus on Catalysts. *Resources* **2021**, *10*, 93. [[CrossRef](#)]
8. Ruiz-Castillo, P.; Buchwald, S.L. Applications of Palladium-Catalyzed C-N Cross-Coupling Reactions. *Chem. Rev.* **2016**, *116*, 12564–12649. [[CrossRef](#)]
9. Palo, E.; Salladini, A.; Morico, B.; Palma, V.; Ricca, A.; Iaquaniello, G. Application of Pd-Based Membrane Reactors: An Industrial Perspective. *Membranes* **2018**, *8*, 101. [[CrossRef](#)]
10. Saad, S.; Hassine, L.; Elfahem, W. Hydrogen FBG sensor using Pd/Ag film with application in propulsion system fuel tank model of aerospace vehicle. *Photonic Sens.* **2014**, *4*, 254–264. [[CrossRef](#)]
11. Xu, B.; Chen, Y.; Zhou, Y.; Zhang, B.; Liu, G.; Li, Q.; Yang, Y.; Jiang, T. A Review of Recovery of Palladium from the Spent Automobile Catalysts. *Metals* **2022**, *12*, 533. [[CrossRef](#)]
12. Phan, T.T.V.; Huynh, T.C.; Manivasagan, P.; Mondal, S.; Oh, J. An Up-To-Date Review on Biomedical Applications of Palladium Nanoparticles. *Nanomaterials* **2019**, *10*, 66. [[CrossRef](#)]
13. Izatt, R.M.; Izatt, S.R.; Izatt, N.E.; Krakowiak, K.E.; Bruening, R.L.; Navarro, L. Industrial applications of molecular recognition technology to separations of platinum group metals and selective removal of metal impurities from process streams. *Green Chem.* **2015**, *17*, 2236–2245. [[CrossRef](#)]
14. Wiecka, Z.; Rzelewska-Piekut, M.; Regel-Rosocka, M. Recovery of platinum group metals from spent automotive converters by leaching with organic and inorganic acids and extraction with quaternary phosphonium salts. *Sep. Purif. Technol.* **2022**, *280*, 119933. [[CrossRef](#)]
15. Dong, H.; Zhao, J.; Chen, J.; Wu, Y.; Li, B. Recovery of platinum group metals from spent catalysts: A review. *Int. J. Miner. Process.* **2015**, *145*, 108–113. [[CrossRef](#)]
16. Paiva, A.P.; Piedras, F.V.; Rodrigues, P.G.; Nogueira, C.A. Hydrometallurgical recovery of platinum-group metals from spent auto-catalysts—Focus on leaching and solvent extraction. *Sep. Purif. Technol.* **2022**, *286*, 120474. [[CrossRef](#)]
17. Karim, S.; Ting, Y.-P. Recycling pathways for platinum group metals from spent automotive catalyst: A review on conventional approaches and bio-processes. *Resour. Conserv. Recycl.* **2021**, *170*, 105588. [[CrossRef](#)]
18. Song, L.; Wang, X.; Li, L.; Wang, Z.; Xu, H.; He, L.; Li, Q.; Ding, S. Recovery of palladium(II) from strong nitric acid solutions relevant to high-level liquid waste of PUREX process by solvent extraction with pyrazole-pyridine-based amide ligands. *Hydrometallurgy* **2022**, *211*, 105888. [[CrossRef](#)]
19. Wang, J.; Xu, W.; Liu, H.; Yu, F.; Wang, H. Extractant structures and their performance for palladium extraction and separation from chloride media: A review. *Miner. Eng.* **2021**, *163*, 106798. [[CrossRef](#)]
20. Xiao, Q.; Song, L.; Wang, X.; Xu, H.; He, L.; Li, Q.; Ding, S. Highly efficient extraction of palladium(II) in nitric acid solution by a phenanthroline-derived diamide ligand. *Sep. Purif. Technol.* **2022**, *280*, 119805. [[CrossRef](#)]
21. Sasaki, Y.; Matsumiya, M.; Kinoshita, R. Recovery of Palladium by Extraction-electrodeposition Using *N, N, N', N', N'', N''*-Hexaocetyl-nitrilotriacetamide. *Solvent Extr. Ion Exch.* **2022**, *40*, 606–619.
22. Wang, X.; Song, L.; Li, L.; Wang, Z.; Li, Q.; He, L.; Huang, X.; Ding, S. Extraction and Complexation Investigation of Palladium(II) by a Nitrilotriacetate-Derived Triamide Ligand. *Inorg. Chem.* **2022**, *61*, 13293–13305. [[CrossRef](#)]
23. Sasaki, Y.; Tsubata, Y.; Kitatsuji, Y.; Sugo, Y.; Shirasu, N.; Morita, Y.; Kimura, T. Extraction Behavior of Metal Ions by TODGA, DOODA, MIDOA, and NTAamide Extractants from HNO₃-ton-Dodecane. *Solvent Extr. Ion Exch.* **2013**, *31*, 401–415. [[CrossRef](#)]

24. Iftekhar, S.; Heidari, G.; Amanat, N.; Zare, E.N.; Asif, M.B.; Hassanpour, M.; Lehto, V.P.; Sillanpaa, M. Porous materials for the recovery of rare earth elements, platinum group metals, and other valuable metals: A review. *Environ. Chem. Lett.* **2022**, *20*, 3697–3746. [[CrossRef](#)]
25. Sharma, S.; Krishna Kumar, A.S.; Rajesh, N. A perspective on diverse adsorbent materials to recover precious palladium and the way forward. *RSC Adv.* **2017**, *7*, 52133–52142. [[CrossRef](#)]
26. Sharma, R.K.; Pandey, A.; Gulati, S.; Adholeya, A. An optimized procedure for preconcentration, determination and on-line recovery of palladium using highly selective diphenyldiketone-monothiosemicarbazone modified silica gel. *J. Hazard. Mater.* **2012**, *209–210*, 285–292. [[CrossRef](#)] [[PubMed](#)]
27. Jayakumar, M.; Venkatesan, K.A.; Srinivasan, T.G.; Rao, P.R.V. Studies on the feasibility of electrochemical recovery of palladium from high-level liquid waste. *Electrochim. Acta* **2009**, *54*, 1083–1088. [[CrossRef](#)]
28. Liu, H.; Ning, S.; Li, Z.; Zhang, S.; Chen, L.; Yin, X.; Fujita, T.; Wei, Y. Preparation of a novel silica-based N-donor ligand functional adsorbent for efficient separation of palladium from high level liquid waste. *Sep. Purif. Technol.* **2022**, *296*, 121373. [[CrossRef](#)]
29. Wu, H.; Kim, S.-Y.; Ito, T.; Miwa, M.; Matsuyama, S. One-pot synthesis of silica-gel-based adsorbent with Schiff base group for the recovery of palladium ions from simulated high-level liquid waste. *Nucl. Eng. Technol.* **2022**, *54*, 3641–3649. [[CrossRef](#)]
30. Awual, M.R.; Yaita, T. Rapid sensing and recovery of palladium(II) using *N,N*-bis(salicylidene)1,2-bis(2-aminophenylthio)ethane modified sensor ensemble adsorbent. *Sens. Actuators B Chem.* **2013**, *183*, 332–341. [[CrossRef](#)]
31. Mincke, S.; Asere, T.G.; Verheye, I.; Folens, K.; Vanden Bussche, F.; Lapeire, L.; Verbeken, K.; Van Der Voort, P.; Tessema, D.A.; Fufa, F.; et al. Functionalized chitosan adsorbents allow recovery of palladium and platinum from acidic aqueous solutions. *Green Chem.* **2019**, *21*, 2295–2306. [[CrossRef](#)]
32. Yu, Q.; Ning, S.; Zhang, W.; Wang, X.; Wei, Y. Recovery of scandium from sulfuric acid solution with a macro porous TRPO/SiO₂-P adsorbent. *Hydrometallurgy* **2018**, *181*, 74–81. [[CrossRef](#)]
33. Ning, S.; Zhang, S.; Zhang, W.; Zhou, J.; Wang, S.; Wang, X.; Wei, Y. Separation and recovery of Rh, Ru and Pd from nitrate solution with a silica-based IsoBu-BTP/SiO₂-P adsorbent. *Hydrometallurgy* **2020**, *191*, 105207. [[CrossRef](#)]
34. Su, Z.; Ning, S.; Li, Z.; Zhang, S. High-efficiency separation of palladium from nitric acid solution using a silica-polymer-based adsorbent isoPentyl-BTBP/SiO₂-P. *J. Environ. Chem. Eng.* **2022**, *10*, 107928. [[CrossRef](#)]
35. Chen, L.; Zhang, J.; He, X.; Liu, M.; Wei, Q.; Wang, X.; Wei, Y. Fast recovery of lead from hydrochloric acid via a novel silica-supported anion exchange resin for the determination of ²¹⁰Pb in environmental samples. *Chem. Eng. J.* **2020**, *396*, 125300. [[CrossRef](#)]
36. Wei, Y.; Kumagai, M.; Takashima, Y.; Modolo, G.; Odoj, R. Studies on the Separation of Minor Actinides from High-Level Wastes by Extraction Chromatography Using Novel Silica-Based Extraction Resins. *Nucl. Technol.* **2017**, *132*, 413–423. [[CrossRef](#)]
37. Ning, S.; Wang, X.; Liu, R.; Wei, Y.; He, L.; Tang, F. Evaluation of Me₂-CA-BTP/SiO₂-P adsorbent for the separation of minor actinides from simulated HLLW. *J. Radioanal. Nucl. Chem.* **2015**, *303*, 2011–2017. [[CrossRef](#)]
38. Wei, Y.Z.; Hoshi, H.; Kumagai, M.; Asakura, T.; Morita, Y. Separation of Am(III) and Cm(III) from trivalent lanthanides by 2,6-bis(triazinyl)pyridine extraction chromatography for radioactive waste management. *J. Alloys Compd.* **2004**, *374*, 447–450. [[CrossRef](#)]
39. Wei, Y.; Wang, X.; Liu, R.; Wu, Y.; Usuda, S.; Arai, T. An advanced partitioning process for key elements separation from high level liquid waste. *Sci. China Chem.* **2012**, *55*, 1726–1731. [[CrossRef](#)]
40. Andelescu, A.; Nistor, M.A.; Muntean, S.G.; Rădulescu-Grad, M.E. Adsorption studies on copper, cadmium, and zinc ion removal from aqueous solution using magnetite/carbon nanocomposites. *Sep. Sci. Technol.* **2018**, *53*, 2352–2364. [[CrossRef](#)]
41. Ianăși, C.; Picioruș, E.-M.; Nicola, R.; Putz, A.-M.; Negrea, A.; Ciopec, M.; Len, A.; Almásy, L. Synthesis and characterization of magnetic iron oxide—Silica nanocomposites used for adsorptive recovery of palladium (II). *Soft Mater.* **2022**, *20*, S68–S75. [[CrossRef](#)]
42. Sasaki, Y.; Tsubata, Y.; Kitatsuji, Y.; Morita, Y. Novel Soft–Hard Donor Ligand, NTAamide, for Mutual Separation of Trivalent Actinoids and Lanthanoids. *Chem. Lett.* **2013**, *42*, 91–92. [[CrossRef](#)]

Disclaimer/Publisher’s Note: The statements, opinions and data contained in all publications are solely those of the individual author(s) and contributor(s) and not of MDPI and/or the editor(s). MDPI and/or the editor(s) disclaim responsibility for any injury to people or property resulting from any ideas, methods, instructions or products referred to in the content.